Available online at www.sciencedirect.com

jmr&t Journal of Materials Research and Technology

journal homepage: www.elsevier.com/locate/jmrt

A computational study of the effect of external heat flux and electric field on the nano-pumping of C_{20} molecules in carbon nanotubes by molecular dynamics simulation

Yupeng Xie [a,**], *Mohammed Al-Bahrani* [b], *Navid Nasajpour-Esfahani* [c], *Dheyaa J. Jasim* [d], *Maboud Hekmatifar* [c], *Shadi Esmaeili* [e], *Fay Fathdal* [f], *Salah Hassan Zain Al-Abdeen* [g], *Davood Toghraie* [c,*], *Malak Jaafar Ali* [g]

[a] *College of Science, Jilin Institute of Chemical Technology, Jilin, 132022, Jilin, China*
[b] *Chemical Engineering and Petroleum Industries Department, Al-Mustaqbal University College, Babylon, 51001, Iraq*
[c] *Department of Mechanical Engineering, Khomeinishahr Branch, Islamic Azad University, Khomeinishahr, Iran*
[d] *Department of Petroleum Engineering, Al-Amarah University College, Maysan, Iraq*
[e] *Faculty of Physics, Semnan University, P.O. Box, 35195-363, Semnan, Iran*
[f] *College of Medical Techology, Al-Farahidi University, Iraq*
[g] *Department of Medical Laboratory Technics, AlNoor University College, Nineveh, Iraq*

ARTICLE INFO

Article history:
Received 28 October 2022
Accepted 1 June 2023
Available online 5 June 2023

Keywords:
Nano-pumping
Carbon nanotube
Fullerene
Molecular dynamics
Atomic modelling
Heat flux effect

ABSTRACT

Nano-pump is a breakthrough that allows a tiny pump to transfer mass inside the atomic channels. These nanostructures can be used in various applications, such as drug delivery systems in clinical cases. Carbon nanotube (CNT) performance as a nano-pump sample was introduced here. For this purpose, Molecular Dynamics (MD) approach, and external heat flux/electric field effect on nano-pump performance were reported. Hence, various physical parameters, such as nano-pumping time, potential/kinetic energy, stress and entropy were reported to describe the nano-pumping performance of CNT samples. Technically, nano-pumping performance was detected by fullerene (C_{20}) molecule displacement inside the NT. The MD outputs indicated by the heat flux implemented inside CNT, nano-pumping process effectively occur. The results show that by increasing the heat flux amplitude ratio from 0.1 to 0.5 W/m^2, the displacement time of C_{20} molecule decreased from 7.49 to 6.96 ps. By amplitude enlarging, the kinetic energy of defined sample converged to 5.70014 eV. This procedure caused more atomic collisions inside the NT, and the nano-pumping process occurred in a smaller time. Furthermore, the electric field caused the nano-pumping process to be delayed in modeled systems. Numerically, by increasing the electric field, the nano-pumping process occurred after 7.85 ps. Increasing the electric field decreased the mechanical wave produced via Cu tip oscillation. This evolution caused the atomic force, and stress on the target particle converged to a lesser value, and the lattice stress value of modeled sample reached 2.12662 $\times$ 10^6 bar.

* Corresponding author.
** Corresponding author.
E-mail addresses: xieyupeng1981@163.com (Y. Xie), Toghraee@iaukhsh.ac.ir (D. Toghraie).
https://doi.org/10.1016/j.jmrt.2023.06.001

1. Introduction

Carbon has many derivatives with different applications in different area [1–6]. One of the most important derivatives of carbon, which has received a lot of attention in the economy and technology, is carbon nanotubes (CNTs) which were used in different applications [1–3]. These NT, hollow cylinders of carbon atoms, were first produced in 1992 by two researchers [7]. CNTs are carbon allotropes consisting of fullerene and graphene, which are divided into single-walled CNTs (SWCNTs) and multi-walled CNTs (MWCNTs) categories based on the number of their graphic shells. By increasing the science and technology, carbon NTs were studied and used more and more in the electrical, physical, chemical, etc., fields in terms of their unique structure. These carbon NTs had high tensile strength [8], acceptable electrical and thermal conductivity [9–11], high corrosion resistance biocompatibility, etc and used in different appliactions such as oxygen reduction reaction catalysts [12], batteries [13] and etc. Regarding their low toxicity, it was used in the biological systems, drug delivery, and cancer treatment. These NTs can minimize side effects in the field of cancer treatment. These carbon NTs can target specific cells without harming others and destroy them using a lower dose of medicine [14–16]. These NTs have successfully transformed nanotechnology, so that this NT is used in the field of water and air purification [17].

Much research was done on CNTs, and their many applications, some of which are discussed below. For instance, Talla et al. [18] investigated the effect of doping on the pristine double-walled boron nitride NTs and evaluated them in different situations. This study's results showed that in the doped double-walled boron nitride NTs, the electronic properties depend on the doping location. Shao et al. [19] created Na+ and K+ hydration process using the molecular dynamics (MD) simulation method. This process happened inside CNT at a temperature of 298 K. The research's results on five CNT structures made it clear that the narrow CNT structures with the diameters of 0.60 and 0.73 nm were the most favourable energy to confining a hydrated K^+ inside. While the situation inside wide CNTs with the diameters of 0.87, 1.0 and 1.28 nm showed the opposite results. Marinall'ina et al. [19] showed that the concentration of pyrrolic nitrogen determined the unusual piezoelectric properties of CNTs doped with nitrogen using the MD method. This study showed that the increase in the concentration of pyrrolic nitrogen had a direct relationship with the magnitude of the piezoelectric strain coefficient of CNTs, and the magnitude of current produced during the deformation of CNTs. Rather et al. [20] studied the hydrogen storage of purified MWCNTs and Ti-decorated MWCNTs. This study shows that the storage improvement process in the composite hydrogen was 13 and 15 times higher than in the virgin sample. Eyvazian et al. [21] examined the effect of geometrical parameters, such as diameter, length and chirality on mechanical properties of CNT structure using a combined MD, and finite element method. The results showed that in examining the structure due to the elasticity, the diameter of NT had a greater effect on the structure than the length of NT. Su et al. [22] examined the transportation of different nanoparticles inside a nanochannel with a hydrophobic-hydrophilic coating by the MD simulation. The results show that the cationic nanoparticles had a higher diffusion coefficient than the anionic nanoparticles. Su et al. [23] examined the transportation of different nanoparticles and ions inside a nanochannel by the MD simulation. The results show that increasing the salt concentration could affect the transportation of nanoparticles. As the external field increased, the ion flux increased and the nanoparticles flux decreased. Su et al. [24] examined the transportation of nanoparticles inside a polymer nanochannel by the MD simulation. The results show that the transfer time of nanoparticles inside the nanochannel becomes longer by increasing in the length of polymer. They showed that as the amount of charge increased, the nanoparticles flux increased.

In the previous articles, some of the numerous properties of CNTs were stated. The present study investigated the effect amplitude of heat flux and electric field on the nano-pumping process in CNTs. To study the nano-pumping performance of C_{20} molecules, the change in lattice stress, potential energy, entropy, kinetic energy, and displacement time of C_{20} molecules was studied. For this purpose, the amplitude of heat flux was considered at 0.1,0. 2, 0.3, and 0.5 W/m^2 magnitude. Moreover, the external electric field was considered with 0.02, 0.04, 0.0.6, 0.08, and 0.10 V/Å magnitude.

2. Simulation and method

2.1. *Molecular dynamics*

The nature of a substance can be studied by searching the structure, and movement of its components. On the other hand, only stable compounds (structures) under present conditions can be analyzed using the experimental techniques. In contrast, computational methods go one step further and can analyze unstable compounds and even compounds that are still unknown. Therefore, the MD method is used, a widely used computational analysis method in chemistry, physics, biology and other experimental sciences [25]. More precisely, the MD method is a computer-dependent method that can analyze the physical movement of atoms and molecules. In this method, a position can be created for the atoms that make up a system so that these atoms can interact with each other for a certain period. Hence, molecular systems should generally consist of many particles. Therefore, the characteristics of complex systems cannot be analytically obtained. But, molecular dynamics simulation

has solved this problem using the computational method. MD method performs the analysis process as a step-by-step numerical solution of Newton's equation of motion in a molecular system. It uses Newton's second law to find the path of the movement of particles relative to real-time. Newton's second law is explained below.

$$F = ma = m\frac{dV}{dt} = m\frac{d^2\boldsymbol{r}}{dt^2} \tag{1}$$

In Eq. (1), r, F *a*, and m shows the position of each atom, the force acting on each atom, the acceleration of each atom, and the mass, respectively. Moreover, the force used to the particles can be obtained via the potential function in the form of Eq. (2).

$$F = -\frac{dU(r)}{dr} \tag{2}$$

The difference between this equation, and previous equation is that in this equation, the force applied to the particles depended on the position of atoms in each other in addition to the potential energy. In Eq. (2), U(r) showed the force field of all potential energy equations. In the previous part of this review, it was found that the force applied to the particles caused them to move from their initial position. The particle movement pattern and displacement rate were studied in this part of MD method. In the MD method, the analytical description of particle motion was not an impossible process, but a difficult process. This process was done using the velocity-Verlet algorithm, one of the most common integral methods of Newton's equations of motion. This algorithm, an integral method, calculated the displacement rate of particles in the MD method using two Taylor series. The velocity-Verlet algorithm is as follows [26–28]:

$$r(t+\Delta t) = r(t) + \Delta t\, v(t) + \frac{\Delta t^2 a\,(t)}{2} \tag{3}$$

$$v(t+\Delta t) = v(t) + \Delta t\, v(t) + \frac{\Delta t\,(a\,(t) + a(t+\Delta t))}{2} \tag{4}$$

In the previous part of this issue, it was stated that the molecular structure consisted of an infinite number of particles that exerted force on each other based on their position. In this part of the MD method, which was the longest part of the MD method due to calculation, the effect of the force of particles on each other was studied. The calculation of interatomic forces is often done using a mathematical function, and the results of this study were compared with the experimental characteristics. Lennard-Jones (LJ) potential and Tersoff studied the interaction among the particles [29–31]. LJ potential function is a simple mathematical model. This potential function described the interaction between two particles (atoms or molecules). This function is displayed below [31]:

$$U_{LJ} = 4\varepsilon\left[\left(\frac{\sigma}{r}\right)^{12} - \left(\frac{\sigma}{r}\right)^{6}\right] \tag{5}$$

In Eq. (5), ε_{ij} is the depth of potential, σ_{ij} is the diameter of particles above which the potential became zero, and r is the distance of the particles from each other. The equations that determined the values of ε_{ij} and σ_{ij},respectively are given below.

Table 1 – The values of ε_{ij} and σ_{ij} coefficients for all present particles [32,33].

Particle's type	ε (kcal/mol)	σ (Å)
C	0.105	3.851
Cu	0.005	3.495

$$\varepsilon_{ij} = \sqrt{\varepsilon_i \varepsilon_j} \tag{6}$$

$$\sigma_{ij} = \frac{\sigma_i + \sigma_j}{2} \tag{7}$$

The values of ε_{ij} and σ_{ij} coefficients for all present particles are reported in Table 1.

In this part, we will examine Tersoff potential, which is the most suitable for carbon and silica particles. The Tersoff potential function is shown below [34]:

$$E = \frac{1}{2}\sum_i \sum_{j\neq i} U_{ij} \tag{8}$$

$$U_{ij} = f_C(r_{ij})\left[a_{ij} f_R(r_{ij}) + b_{ij} f_A(r_{ij})\right] \tag{9}$$

This potential consists of three terms: f_A (repellent

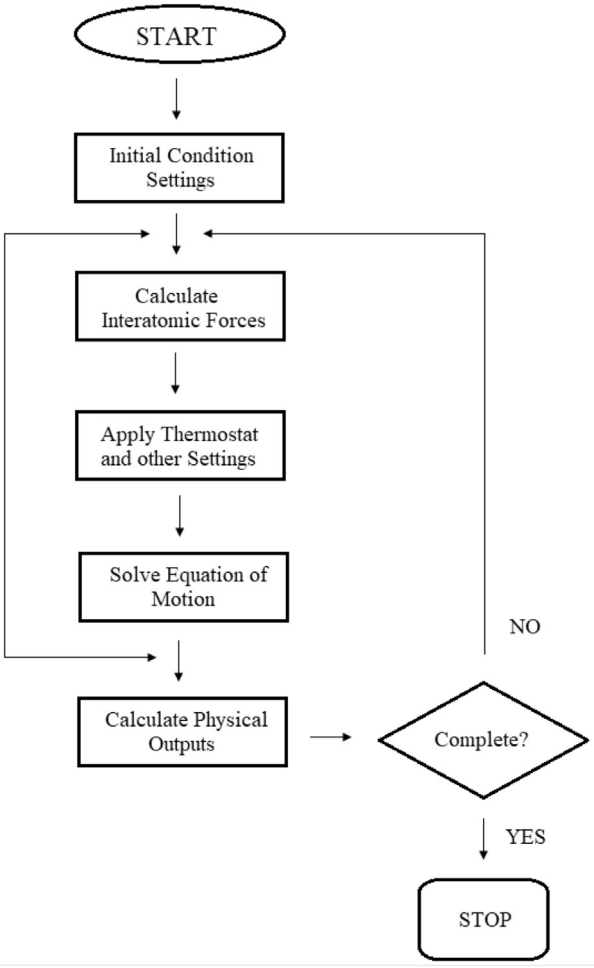

Fig. 1 – Computational algorithm in current computational research.

interaction), f_R (absorbent interaction), and $f_c(r)$. In the following, the overall shape of this structure was studied.

$$f_R(r) = A\exp(-\lambda_1 r) \tag{10}$$

$$f_A(r) = -B\exp(-\lambda_2 r) \tag{11}$$

$$f_C(r) = \begin{cases} 1 & r < R - D \\ \frac{1}{2} - \frac{1}{2}\sin\left(\frac{\pi}{2}\frac{r-R}{D}\right) & R - D < r < R + D \\ 0 & r > R + D \end{cases} \tag{12}$$

where, A, B, λ_1, and λ_2 are the potential constants. Our used algorithm in current research is depicted in Fig. 1. Computationally, our MD outputs are calculated 5 times by this computational algorithm, and the average ratio of them is reported. So, we can say the computational errors in current simulations are excluded from our research.

2.2. Simulation details

In this part of the present study, the details of MD simulation are discussed. These structures were modeled by various software under initial hypothetical conditions, such as a time step of 1 fs, simulation time of 8 ps and initial temperature of 300 K in a simulation box with the dimensions of $60 \times 80 \times 210$ nm^3. CNT was modeled with a zigzag edge, a length of 134 nm, and a diameter of 10 nm using VMD

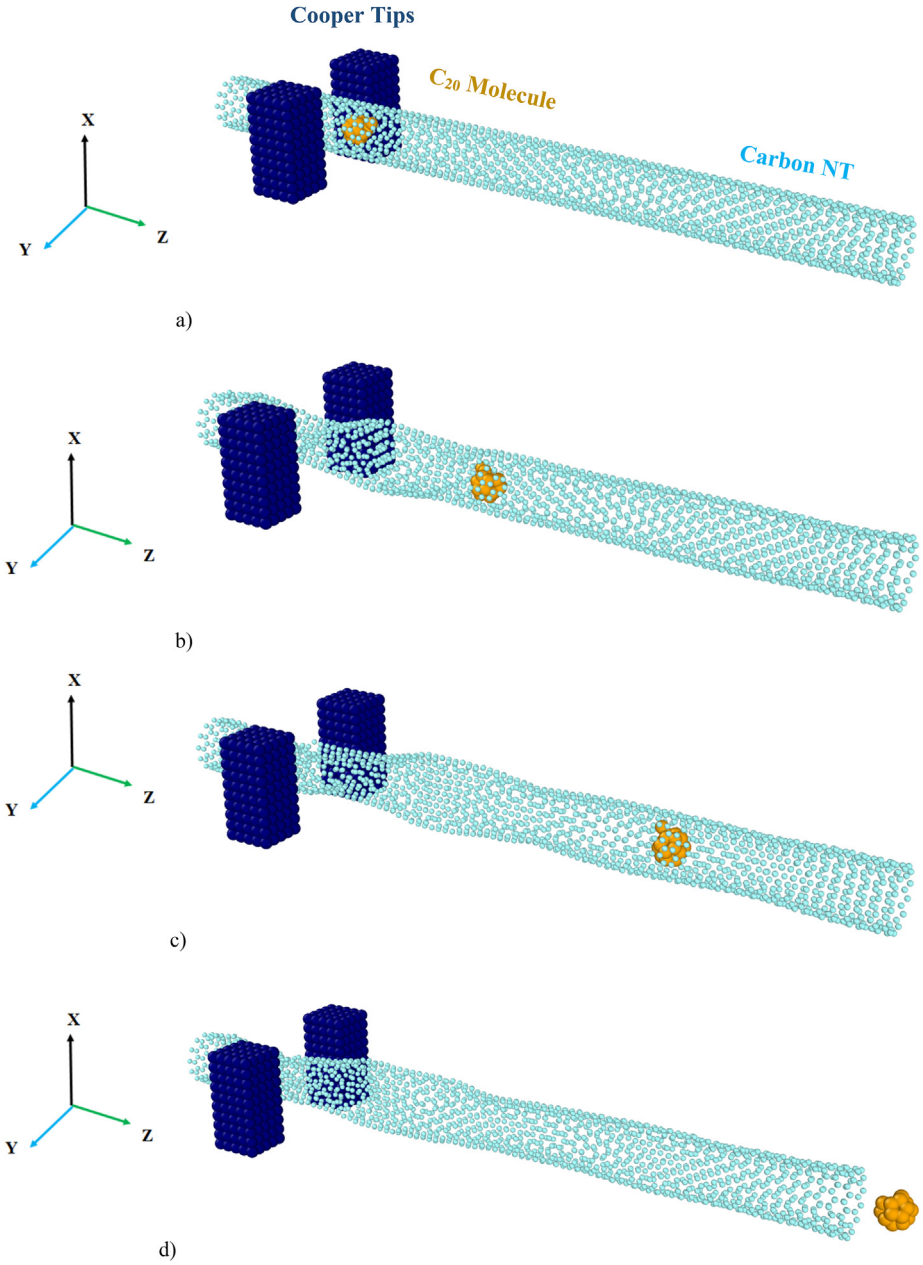

Fig. 2 – A schematic of the nano-pumping process at a) 0, b) 2.5, c) 5, d) 7.5 ps.

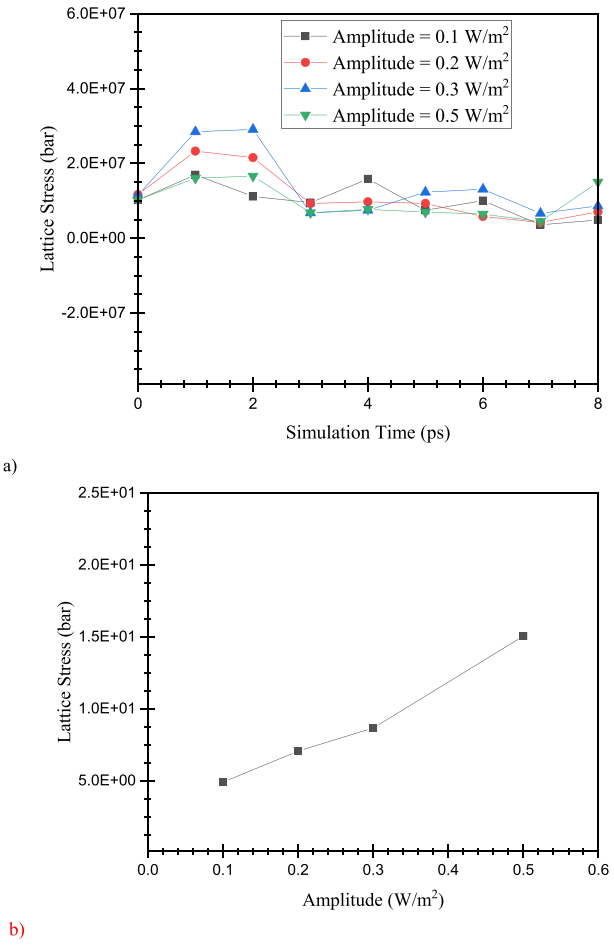

Fig. 3 – The change in lattice stress of C_{20} molecule flux in terms of a) simulation time and b) heat flux amplitude.

software. In the next step, C_{20} molecule was modeled using LAMMPS software. Furthermore, the simulated structures were packed together using Packmol software. Finally, in the last step of modeling the structure, two Tips with cooper type and the dimensions of $8 \times 8 \times 20$ nm^3 were modeled on both sides of the NT (Y-direction). The boundary conditions are periodically considered in all directions, and the temperature of simulated structure was controlled using NVT ensemble and Nose-Hoover thermostat. A schematic of the nano-pumping process is represented in Fig. 2.

In the following, the nano-pumping process was studied in the presence of external heat flux with different amplitudes (with 0.1,0. 2, 0.3, and 0.5 W/m^2 magnitudes), and frequency of 10 ps^{-1}. Technically, we used 'fix heat' command in the LAMMPS package. This setting in all simulations added non-translational kinetic energy (heat) to a group of atoms in a manner that conserved their aggregate momentum [35]. Finally, the external electric fields with 0.02, 0.04, 0.0.6, 0.08, and 0.10 V/Å magnitude were considered to study the nano-pumping process.

Table 2 – The change in lattice stress, potential energy, and entropy of structures with increasing amplitude of external heat flux.

Amplitude (W/m^2)	Lattice Stress (10^6 bar)	Potential energy (eV)	Entropy (eV/K)
0.1	4.89643	−110.18001	412.27935
0.2	7.05342	−109.93102	411.42874
0.3	8.66073	−109.6423	405.82218
0.5	15.0492	−109.34472	401.87414

3. Results and discussion

3.1. *The effect of EHFF*

This part studied the effect of variable heat flux amplitude on the nano-pumping process of C_{20} molecule in the CNT. Cu tips in this arrangement caused mechanical wave production inside the NT and C_{20} molecule as target mass displaced. Moreover, external heat flux with various amplitudes was inserted inside the MD box. The amplitude ratio of this external parameter varied from 0.1 to 0.5 W/m^2, and the nano-pumping performance of defined atom-base system was

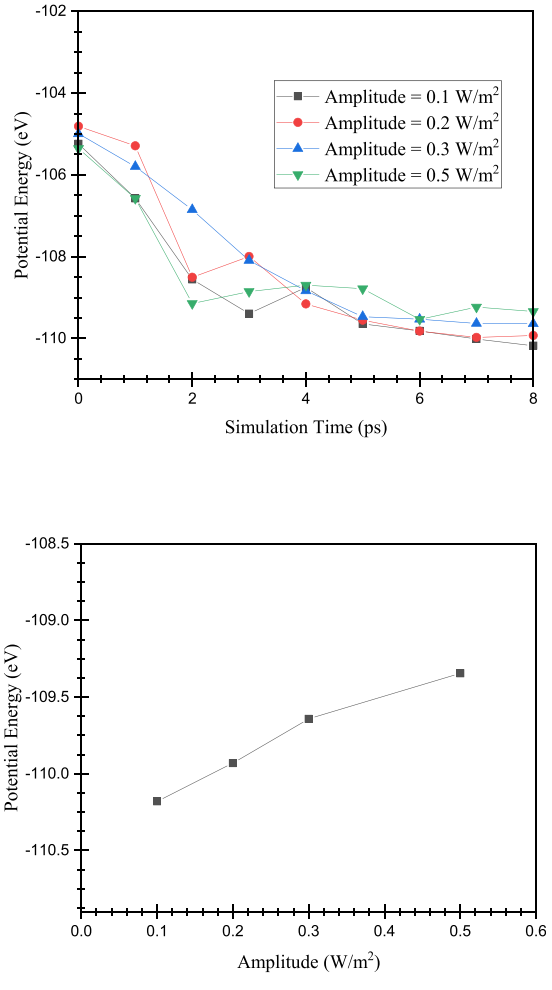

Fig. 4 – The change in potential energy of C_{20} molecule in terms of a) simulation time and b) heat flux amplitude.

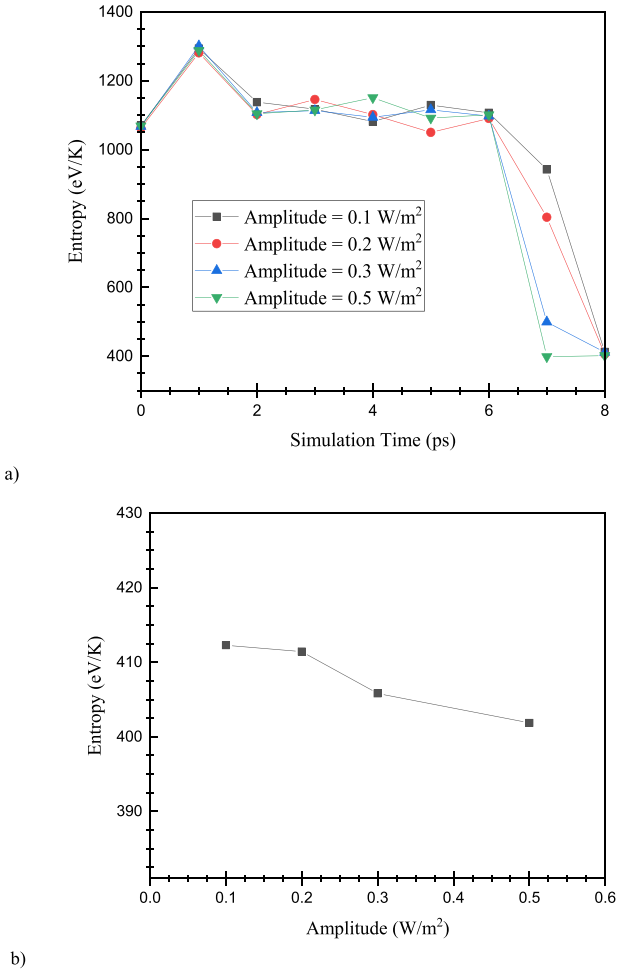

Fig. 5 – The change in entropy of the C_{20} molecule in terms of a) simulation time and b) heat flux amplitude.

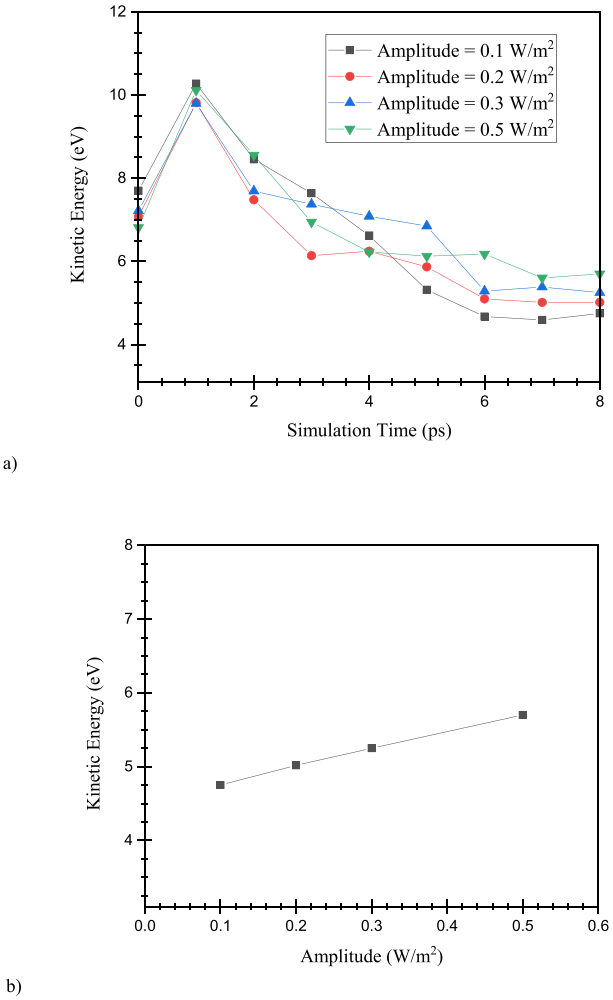

Fig. 6 – The change in the kinetic energy of the C_{20} molecule in terms of a) simulation time and b) heat flux amplitude.

described. Amplitude enlarging caused more atomic collisions inside the NT and the nano-pumping process occurred in a smaller time. The MD outputs predicted atomic stress increased by amplitude enlarging. Fig. 3 shows the change in lattice stress of C_{20} molecule by increasing amplitude of external heat flux. This evolution caused C_{20} molecule to be effectively pushed inside atomic tube. Numerically, the lattice stress parameter's maximum ratio reached 15.0492×10^6 bar in the designed process. Our calculated results in this computational step are reported in Table 2.

Potential energy changes of modeled samples as a function of heat flux amplitude are reported in Fig. 4. As shown in this figure, the potential energy converged to a negative ratio by increasing the amplitude. This atomic performance arose from the atomic fluctuation increasing of target molecule inside the MD box. Potential energy changes in the modeled atomic systems can analyze this type of particle-base evolution. As shown in Fig. 4, external heat flux caused the potential energy of simulated compounds to converge to a larger negative ratio. This performance caused a larger interatomic force to be inserted into particles and displaces of defined fullerene molecule in a smaller time. Numericlly, the maximum ratio of potential energy converged to −109.34 eV. This described process caused the atomic mobility of samples

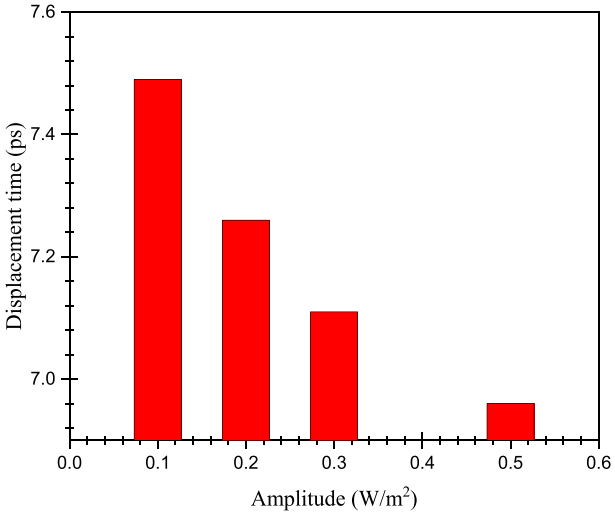

Fig. 7 – The change in displacement time of C_{20} molecule by increasing amplitude of external heat flux.

Table 3 – The change in kinetic energy and displacement time of C_{20} molecule by increasing amplitude of external heat flux.

Amplitude (W/m^2)	Kinetic energy (eV)	Displacement time (ps)
0.1	4.74984	7.49
0.2	5.01717	7.26
0.3	5.24852	7.11
0.5	5.70014	6.96

increases. But, the physical stability of the CNT-C_{20} system didn't decrease, and the introduced procedure could be implemented in actual applications.

The entropy changes of samples are reported in Fig. 5. From this calculation, we can say the entropy and disorder of compounds did not effectively change by heat flux inserting inside the MD box, and this parameter converged to 401.87 eV/K numerical outputs in this section are reported in Table 1. This calculation showed CNT-C_{20} samples promising performance for the mass transfer process in actual cases.

The increasing atomic mobility can be described by nano-pumping time and kinetic energy variation. Fig. 6 shows this parameter changes as a function of heat flux amplitude. The defined sample's kinetic energy converged to 5.70014 eV by enlarging amplitude to 0.5 W/m^2. By this atomic evolution occurred, mass transfer was effectively detected. Physically, the kinetic energy of fullerene molecules arose from the atomic collision between buck ball and CNT systems.

The time of nano-pumping clearly showed the heat flux effect on the defined process. The displacement time of C_{20} molecule changes as a function of external heat flux and simulation time depicted in Fig. 7. Our calculated ratios predicted C_{20} molecule exited from ideal CNT after 6.96 ps by heat flux amplitude increasing to 0.5 W/m^2. This time ratio was consistent with previous reports and validates our numerical method settings in this research [36,37]. As shown in Fig. 7, this time was sufficient for the displacement of C_{20} molecules. So, we can say that nano-pumping performance for industrial/clinical purposes on a nano-scale can be improved by heat flux inserted into a pristine system. Our numerical results for kinetic energy and nano-pumping time as a function of heat flux are listed in Table 3.

3.2. *The effect of increasing electric field*

The results show that the nano-pumping process had the best performance in variable heat flux with an amplitude of 0.5 W/

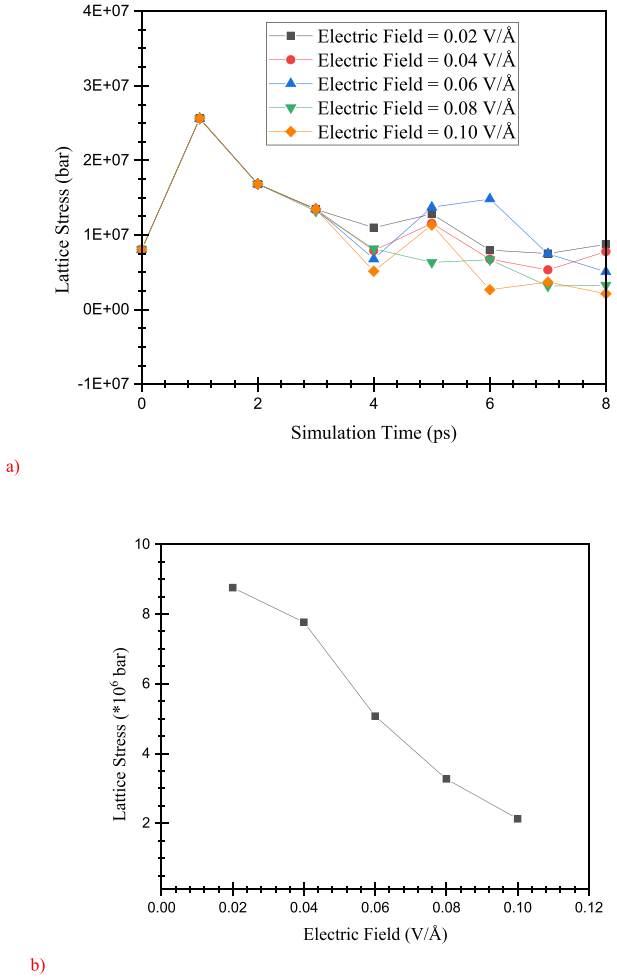

Fig. 8 – The change in lattice stress of the C_{20} molecule in terms of a) simulation time and b) electric field.

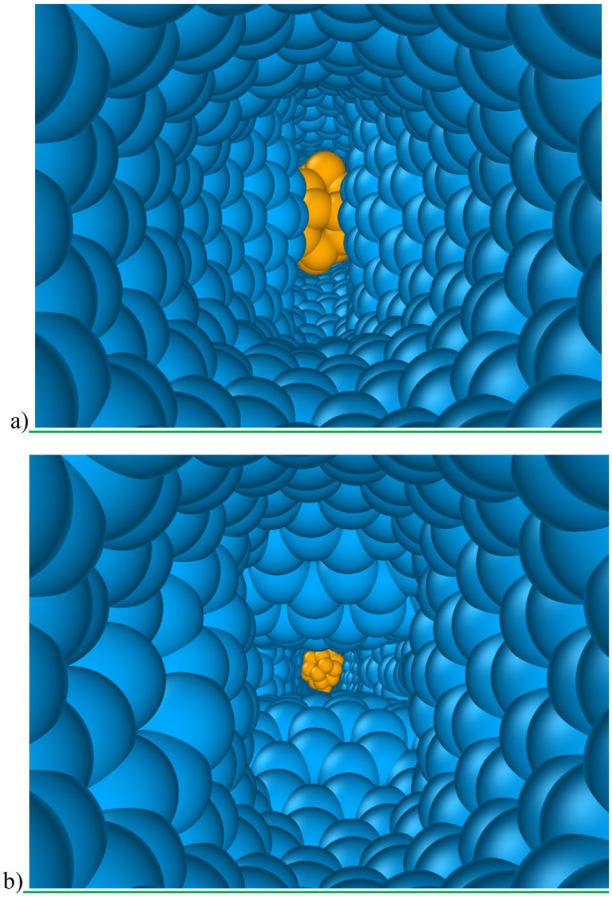

Fig. 9 – The atomic arrangement changes in defined system a) before and b) after 3 ps in presence of 0.1 eV electric field.

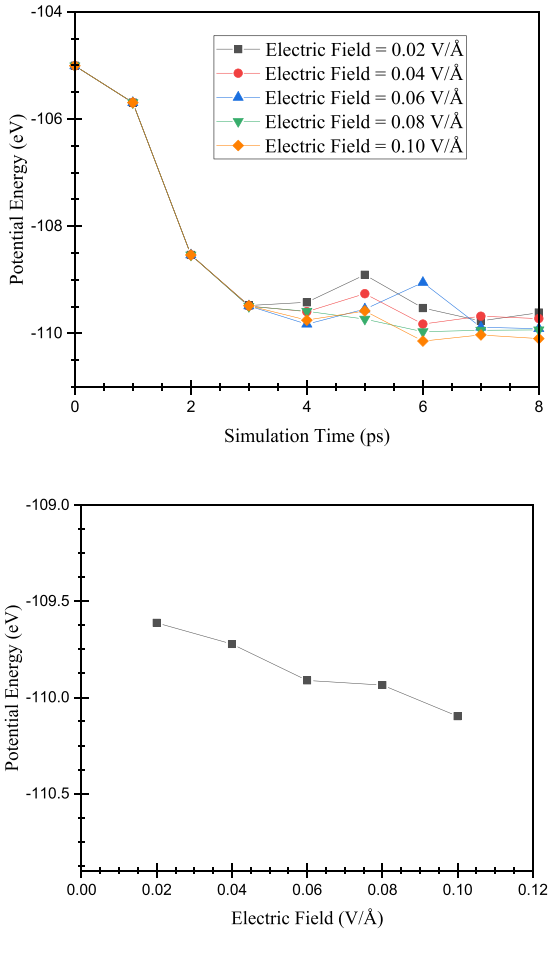

Fig. 10 – The change in potential energy of the C_{20} molecule in terms of a) simulation time and b) electric field.

m^2. In the following, the effect of electric field in the presence of heat flux (with amplitude = 0.5 W/m^2) was studied. The external electric field was used with 0.02, 0.04, 0.0.6, 0.08, and 0.10 V/Å magnitude. Fig. 8 shows the change in lattice stress of C_{20} molecule by increasing the electric field. Increasing the electric field decreased the mechanical wave produced via Cu Tips oscillation. This evolution caused the atomic force and lattice stress on the target particle to converge to a lesser value, and the stress value of modeled sample decreased to 2.12662×10^6 bar. Structurally, after 3 ps, electric field caused atomic arrangement of modeld system changes effectively. Our modeled sample change before/after 3 ps depicted in Fig. 9. This atomic arrangement changes, caused energy of atom-base structure converged to various ratio. So, this described procedure caused net force which implemented to target molecule from nanotube changed and nano-pumping process occur in various intensity.

Furthermore, the physical stability of modeled samples was described by potential energy estimation. Fig. 10 represents the change in the potential energy of C_{20} molecule by increasing electric field. The MD outputs showed the potential energy of samples increased by the electric field increases. The potential energy converged to −110.0974 eV in an electric field with a 0.1 V/Å magnitude. This process arose from the

Table 4 – The change in lattice stress, potential energy, and entropy of structures by increasing the electric field.

Electric Filed (V/Å)	Stress (10^6 bar)	Potential energy (eV)	Entropy (eV/K)
0.02	8.76038	−109.61191	405.48949
0.04	7.76756	−109.72249	406.32566
0.06	5.0713	−109.91133	407.26806
0.08	3.26794	−109.93534	408.26557
0.10	2.12662	−110.0974	409.88801

interaction ratio decreasing by an atom missing from the ideal NT. Our simulations in this step indicated electric field caused the nano-pumping process to occur with lesser efficiency. The numerical results are reported in Table 4.

The entropy of defined samples was calculated for more physical analysis of CNT-C_{20} system in current computational research. Fig. 11 represents the change in entropy of C_{20} molecule by increasing the electric field. By the electric field increasing to 0.1 V/Å, the system's entropy converged to 409.88801 eV/K. As shown in this figure, the electric field didn't change the entropy of the sample appreciably, and the destruction of atomic arrangement didn't occur.

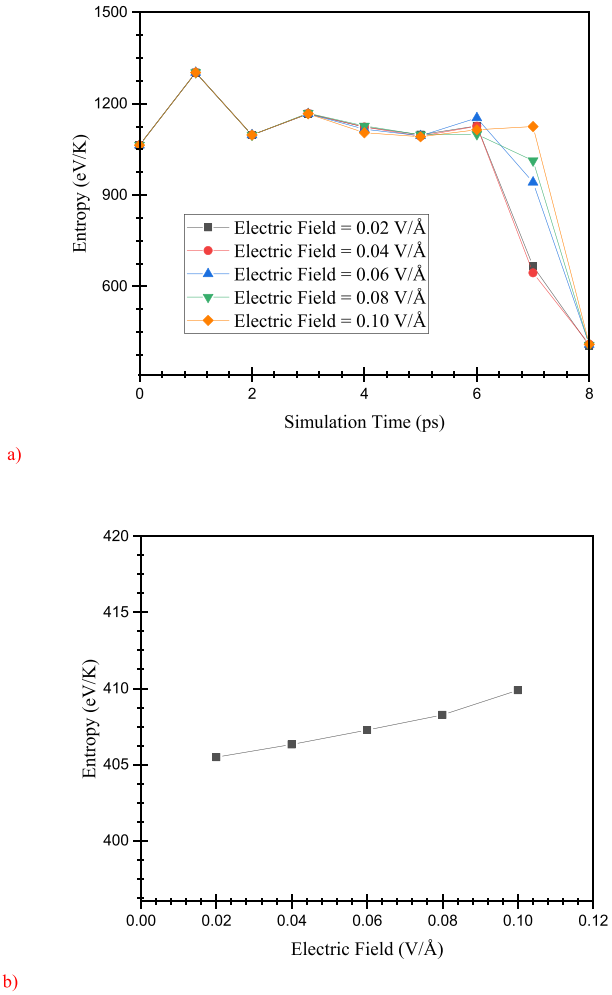

Fig. 11 – The change in entropy of the C_{20} molecule in terms of a) simulation time and b) electric field.

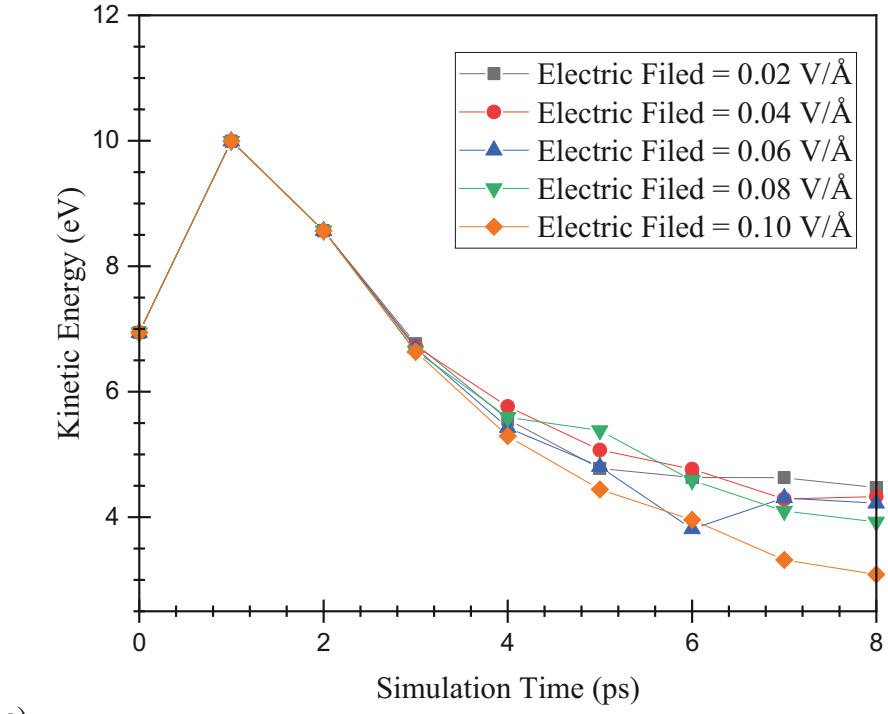

a)

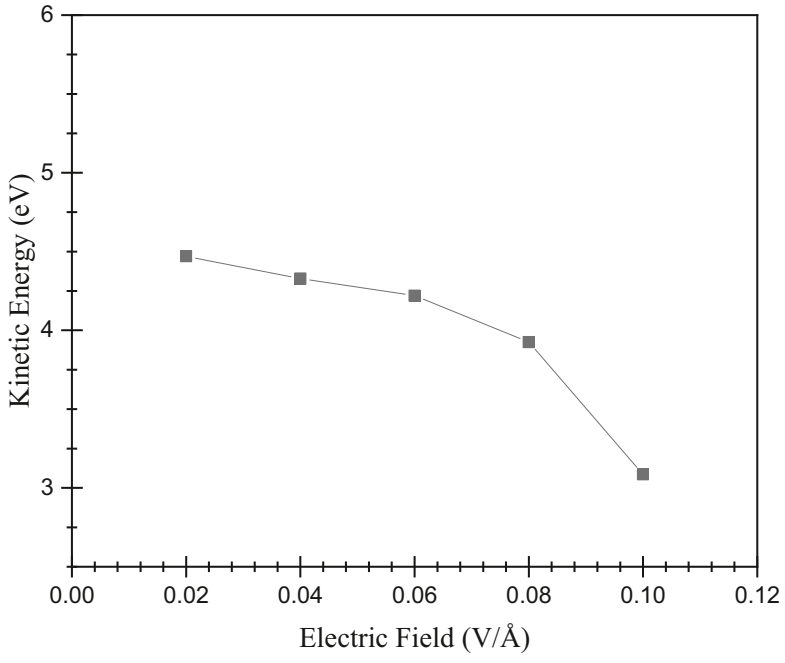

b)

Fig. 12 – The change in the kinetic energy of the C_{20} molecule in terms of a) simulation time and b) electric field.

To analyze the nano-pumping process of CNT-C_{20} system in the presence of an external electric field, the sample's kinetic energy was calculated. Kinetic energy outputs are depicted in Fig. 12. As shown in this figure, by external fields enlarging, the kinetic energy of C_{20} molecule decreased and reached 3.09 eV. Physically, this numerical decrease arose from atomic collision decreasing inside the NT structure. So, we concluded lesser mechanical energy was inserted into the C_{20} molecule by external field enlarging. Finally, this procedure caused fullerene molecules exiting from the pristine NT to be delayed and occurred in more MD time.

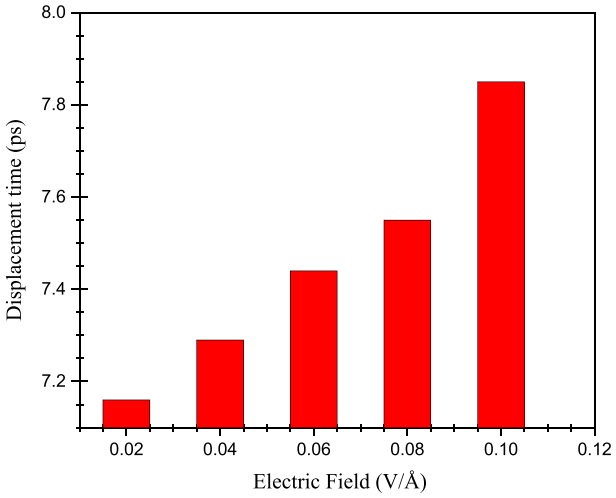

Fig. 13 – The change in displacement time of the C_{20} molecule by increasing the electric field.

Table 5 – The change in kinetic energy and displacement time of C_{20} molecule by increasing the electric field.

Electric Field (V/Å)	Kinetic energy (eV)	Displacement time (ps)
0.02	4.47017	7.16
0.04	4.32837	7.29
0.06	4.22064	7.44
0.08	3.92505	7.55
0.10	3.08631	7.85

As reported in Fig. 13 and Table 5, the nano-pumping process was detected after 7.85 ps in the presence of electric field. Technically, MD results in current computational research declared nano-pumping performance manipulated by the external heat flux and electric field changes. So, for actual applications of this system in various fields, one can use external heat flux and electric field to decrease or enlarge the mass transfer process in nano-scales.

4. Conclusion

In this study, the nano-pumping process in CNT structure used the computational simulations as described. Technically, the MD approach was used in the defined initial condition. Cu tips oscillated with finite amplitude to produce nano-pumping evolution to defined CNT. Furthermore, the nano-pumping process was detected by C_{20} molecule displacement inside the computational box. The MD outputs indicated nano-pumping process could be detected in the CNT-C_{20} system. Our main results in this research are listed below.

A. The potential energy of modeled CNT-C_{20} system converged to a finite value. This physical convergence showed the atomic stability of defined compounds. The potential energy of modeled samples converged to −109.34472 and −110.0974 eV by inserting heat flux and electric field inside the MD box.
B. The entropy convergence of various CNT-C_{20} samples showed their physical stability for actual applications.
C. The kinetic energy changes in defined samples caused the nano-pumping process to occur at various times. Physically, this process arose from atomic stress changes by implementing external heat flux and electric field.
D. External heat flux implemented to the samples improved the nano-pumping process. Numerically, the nano-pumping process time decreased to 6.96 ps.
E. Using an electric field with 0.1 V/Å magnitude to NT, the nano-pumping time of CNT increased to 7.85 ps.

These MD outputs showed that external parameters, such as heat flux and electric field are essential to control the CNT nano-pumping process. Therefore, optimizing the nano-pumping process of CNT can be considerably improved for various aims, such as drug delivery procedures in clinical cases.

Declaration of competing interest

The authors declare that they have no known competing financial interests or personal relationships that could have appeared to influence the work reported in this paper.

REFERENCES

[1] Peng JL, et al. The carbon nanotubes-based materials and their applications for organic pollutant removal: a critical review. Chin Chem Lett 2021;32(5):1626–36.
[2] Huang K, Xu Q, Ying Q, Gu B, Yuan W. Wireless strain sensing using carbon nanotube composite film. Compos B Eng 2023;256:110650.
[3] Wang Z, Dai L, Yao J, Guo T, Hrynsphan D, Tatsiana S, et al. Enhanced adsorption and reduction performance of nitrate by Fe–Pd–Fe_3O_4 embedded multi-walled carbon nanotubes. Chemosphere 2021;281:130718.
[4] Du S, Xie H, Yin J, Sun Y, Wang Q, Liu H, et al. Giant hot electron thermalization via stacking of graphene layers. Carbon 2023;203(25):835–41.
[5] Qiu C, Jiang L, Gao Y, Sheng L. Effects of oxygen-containing functional groups on carbon materials in supercapacitors: a review. Mater Des 2023;230:111952.
[6] Wan S, et al. Co/N-doped carbon nanotube arrays grown on 2D MOFs-derived matrix for boosting the oxygen reduction reaction in alkaline and acidic media. Chin Chem Lett 2021;32(2):816–21.
[7] Iijima S. Nature (london) 354 56 crossref google scholar ebbesen TW and ajayan PM 1992. Nature (London) 1991;358:220.
[8] Moniruzzaman M, Winey KI. Polymer nanocomposites containing carbon nanotubes. Macromolecules 2006;39(16):5194–205.
[9] Mintmire JW, Dunlap BI, White CT. Are fullerene tubules metallic? Phys Rev Lett 1992;68(5):631.
[10] Tans S, Devoret M, Dai H, Thess A, Smalley RE, et al. Individual single-wall carbon nanotubes as quantum wires. Nature 1997;386(6624):474–7.

[11] Kwon Y-K, Kim P. Unusually high thermal conductivity in carbon nanotubes. In: High thermal conductivity materials. Springer; 2006. p. 227–65.
[12] Liu BS, et al. A new strategy to access Co/N co-doped carbon nanotubes as oxygen reduction reaction catalysts. Chin Chem Lett 2021;32(1):535–8.
[13] Zong LB, et al. Stable confinement of Fe/Fe3C in Fe, N-codoped carbon nanotube towards robust zinc-air batteries. Chin Chem Lett 2021;32(3):1121–6.
[14] Scannell JW, Blanckley A, Boldon H, Warrington B. Diagnosing the decline in pharmaceutical R&D efficiency. Nat Rev Drug Discov 2012;11(3):191–200.
[15] He H, Liang Q, Shin MC, Lee K, Gong J, et al. Significance and strategies in developing delivery systems for bio-macromolecular drugs. Front Chem Sci Eng 2013;7(4):496–507.
[16] Wouters OJ, McKee M, Luyten J. Estimated research and development investment needed to bring a new medicine to market, 2009-2018. JAMA 2020;323(9): 844–53.
[17] Patil SB, Basavarajappa PS, Ganganagappa N, Jyothi M, Raghu A, Reddy KR. Recent advances in non-metals-doped TiO2 nanostructured photocatalysts for visible-light driven hydrogen production, CO2 reduction and air purification. Int J Hydrogen Energy 2019;44(26):13022–39.
[18] Talla J, Al-Khaza'leh K, Omar N. Tuning the electronic properties of carbon-doped double-walled boron nitride nanotubes: density functional theory. Russ J Inorg Chem 2022:1–10.
[19] Il'ina M, Il'in O, Osotova O, Khubezhov S, Rudyk N, Pankov l, et al. Pyrrole-like defects as origin of piezoelectric effect in nitrogen-doped carbon nanotubes. Carbon 2022;190:348–58.
[20] Rather S-u. Hydrogen uptake of Ti-decorated multiwalled carbon nanotube composites. Int J Hydrogen Energy 2021;46(34):17793–801.
[21] Eyvazian A, Zhang C, Musharavati F, Farazin A, Mohammadimehr M, Khan A. Effects of appearance characteristics on the mechanical properties of defective SWCNTs: using finite element methods and molecular dynamics simulation. The European Physical Journal Plus 2021;136(9):1–24.
[22] Su J, De La Cruz MO, Guo H. Solubility and transport of cationic and anionic patterned nanoparticles. Phys Rev 2012;85(1):011504.
[23] Su J, Guo H. Translocation of a charged nanoparticle through a fluidic nanochannel: the interplay of nanoparticle and ions. J Phys Chem B 2013;117(39):11772–9.
[24] Su J, Yang K, Guo H. Translocation of a nanoparticle through a fluidic channel: the role of grafted polymers. Nanotechnology 2014;25(18):185703.
[25] Zhang L, Xiong D, Su Z, Li J, Yin L, Yao Z, et al. Molecular dynamics simulation and experimental study of tin growth in SAC lead-free microsolder joints under thermo-mechanical-electrical coupling. Mater Today Commun 2022;33:104301.
[26] Rapaport DC, Rapaport DCR. The art of molecular dynamics simulation. Cambridge university press; 2004.
[27] Spreiter Q, Walter M. Classical molecular dynamics simulation with the Velocity Verlet algorithm at strong external magnetic fields. J Comput Phys 1999;152(1):102–19.
[28] Hairer E, Lubich C, Wanner G. Geometric numerical integration illustrated by the Störmer–Verlet method. Acta Numer 2003;12:399–450.
[29] Toghraie D, Hekmatifar M, Salehipour Y, Afrand M. Molecular dynamics simulation of Couette and Poiseuille Water-Copper nanofluid flows in rough and smooth nanochannels with different roughness configurations. Chem Phys 2019;527:110505.
[30] Daw MS, Baskes MI. Embedded-atom method: derivation and application to impurities, surfaces, and other defects in metals. Phys Rev B 1984;29(12):6443.
[31] Lennard-Jones JE. Cohesion. Proc Phys Soc 1931;43(5):461. 1926-1948.
[32] Rappé AK, Casewit CJ, Colwell K, Goddard III WA, Skiff WM. UFF, a full periodic table force field for molecular mechanics and molecular dynamics simulations. J Am Chem Soc 1992;114(25):10024–35.
[33] Berendsen H, Grigera J, Straatsma T. The missing term in effective pair potentials. J Phys Chem 1987;91(24):6269–71.
[34] Tersoff J. New empirical approach for the structure and energy of covalent systems. Phys Rev B 1988;37(12):6991.
[35] https://docs.lammps.org/fix_heat.html.
[36] Li S, Sajadi SM, Alharbi KAM, El-Shorbagy M, Tlili I. The molecular dynamics study of vacancy defect influence on carbon nanotube performance as drug delivery system. Eng Anal Bound Elem 2022;143:109–23.
[37] Shi X, He X, Sun L, Liu X. Influence of defect number, distribution continuity and orientation on tensile strengths of the CNT-based networks: a molecular dynamics study. Nanoscale Res Lett 2022;17(1):1–13.